Electrochimica Acta 407 (2022) 139900

Contents lists available at ScienceDirect

Electrochimica Acta

journal homepage: www.elsevier.com/locate/electacta

Naphthenic acid corrosion of API 5L X70 steel in aqueous/oil environment using electrochemical surface-resolved and analytical techniques

Rejane M.P. Silva[a,b], Hugo B. Suffredini[b], Ivan N. Bastos[c,*], Luis F. Santos[d], Alda M.P. Simões[d]

[a] Instituto de Pesquisas Energéticas e Nucleares, IPEN/CNEN, Av. Prof. Lineu Prestes, 2242, São Paulo SP 05.508-000, Brazil
[b] Universidade Federal do ABC, Centro de Ciências Naturais e Humanas, Rua Santa Adélia, 166, Bairro Bangu, Santo André, SP 09.210-170, Brazil
[c] Instituto Politécnico, Universidade do Estado do Rio de Janeiro, Rua Bonfim, 25, Nova Friburgo, RJ 28.625-570, Brazil
[d] Centro de Química Estrutural, Institute of Molecular Sciences, Departamento de Engenharia Química, Instituto Superior Técnico, Av. Rovisco Pais, 1049-001 Lisboa, Portugal

ARTICLE INFO

Article history:
Received 27 October 2021
Revised 12 January 2022
Accepted 12 January 2022
Available online 14 January 2022

Keywords:
Electrochemical impedance spectroscopy
LEIS
SECM
Naphthenic acid
Corrosion

ABSTRACT

Naphthenic acid corrosion of steel is studied in crude oil/aqueous phase system at ambient temperature, using a biphasic stagnant liquid without emulsification, by means of electrochemical measurements and surface analysis. The *in-situ* electrochemical impedance is assigned to the processes occurring at the aqueous phase. Corrosion occurred only in the region of the aqueous phase, as crater-shaped pits that eventually coalesced, generating a nearly uniform attack in the vicinity of the oil phase. The impedance values, normalized to the aqueous region only, reveal corrosion rate increasing with the ratio of crude oil/water. Despite the localized character of the anodic oxidation, the iron naphthenate corrosion products became partitioned between the two phases. Surface-resolved electrochemical techniques in aqueous solution revealed enhanced activity of the regions pre-exposed to oil.

1. Introduction

Early corrosion failure of steel structures dealing with crude oil/seawater mixtures is commonly induced by naphthenic acids (HNap) [1,2]. Naphthenic acids are chemically defined as a group of aliphatic organic carboxylic acids, containing one or more cyclopentane or cyclohexane rings [3]. They are naturally present in many crude oils, in contents that can go up to *ca.* 3-4 wt.% [4] and constitute an important class of corrosion-inducing contaminants [5]. Naphthenic acid corrosion (NAC) is most relevant under high-temperature operation systems [6–8], namely in distillation columns, where these acids evaporate under the high temperatures and then condensate on the cooler parts of the column walls, causing intense corrosion [9]. Further to the high temperature and low pressure, other factors influence NAC, namely the presence of thin FeS scale films [6] which tends to provide some protection, or the shear stress that tends to remove any films from the surface at the pipe surface [10]. In the corrosion process, iron is oxidised by the naphthenic acids, forming iron naphthenates [2,8,9]. These HNap have great affinity for the oil phase, although the species tend to become partitioned between the water and the oil phases [11,12].

Despite the relevance and research focus on corrosion under simulated industrial conditions, namely high-temperature, low-pressure, and hydrodynamic conditions, questions remain on the corrosion mechanism and on the meaning of electrochemical data obtained in these liquid/liquid systems. Learning about the process occurring under relatively mild conditions is relevant because the moderate corrosion rate allows monitoring of the early corrosion stages. There are few studies reported on NAC at moderate temperature. Rios et al. [13] used *in-situ* techniques and reported the formation of insoluble iron naphthenate on the steel surface on the initial stages of NAC at room temperature. Schütz et al. [14] detected a linear variation of the pitting potential with the concentration of inclusions at the surface in pipeline steel alloys, the correlation being likely dictated by the water-soluble form of the naphthenic acids, which tend to cause corrosion at the interface of FeS inclusions [14,15]. The effect of inclusions was also investigated on stainless steel. By monitoring the fluctuations of current and potential in AISI 316, Hass et al. [15] reported that the

* Correspondence.
E-mail addresses: rejanep2silva@gmail.com (R.M.P. Silva), hugo.suffredini@ufabc.edu.br (H.B. Suffredini), inbastos@iprj.uerj.br (I.N. Bastos), luis.santos@tecnico.ulisboa.pt (L.F. Santos), alda.simoes@tecnico.ulisboa.pt (A.M.P. Simões).

https://doi.org/10.1016/j.electacta.2022.139900
0013-4686/

noise level, and thus the corrosion activity, increased mostly with the temperature but also with the addition of naphthenic acids.

One other aspect discussed in the literature is the composition of emulsions. For an emulsion formed by adding free water to crude oil, Becerra et al. [16] observed an increase of the ohmic resistance with the amount of water, which suggests that the oil may be the corrosive agent while water presents low corrosion of the surface. In a study dealing with carbon steel corrosion under hydrodynamic conditions, Perini et al. reported that, for oil contents below 20 wt%, using mineral oil and a surfactant solution as components of the emulsion, enhanced electrochemical activity was observed when compared to the base surfactant solution [17].

Methods proposed to study naphthenic corrosion are commonly based on mass loss and electrical resistance probes [2,18], and on the electrochemical noise technique [19,20,21]. Electrochemical impedance spectroscopy (EIS) is a powerful technique for high resistive media. EIS has been employed mostly to study the dielectric properties of oil, oil-water emulsions, and industrial lubricants [17,22,23], using inert electrodes and high frequencies, up to 10 MHz. EIS studies involving corrosion, however, require lower frequencies, below 10 kHz. One of the scarce studies in this line combines EIS with the effects of hydrodynamics and mass transfer, by using a rotating disk electrode or a jet impingement electrochemical cell; complemented by other parameters, thus corrosion rates were estimated [16]. Despite these results, the lack of separation between the two phases remains as a limitation in the understanding of the corrosion mechanism and the use of a system with well-defined stagnant phases come as a potentially interesting approach.

Another possible approach involves surface-resolved electrochemical techniques; these open new opportunities for the understanding of surface and interfacial electrochemistry [24,25]. Among the electrochemical probe techniques, the scanning electrochemical microscopy (SECM) has allowed mapping the concentration of dissolved iron and oxygen along the surface of corroding metals [26,27,28,29], whereas localized electrochemical impedance spectroscopy (LEIS) has been applied mostly to the study of galvanic or pitting corrosion [30]. These techniques, however, have been restricted to continuous aqueous phases. The study of corrosion in a biphasic medium is highly challenging and specific strategies are needed to avoid contamination of the electrodes. Our approach involves the measurement of the metal activity, following the exposure to crude oil or to dilute sulfate aqueous solution, with the purpose of understanding the changes on the metal surface resulting from the contact with the oil phase.

Seamless and welded steel pipes for the oil and natural gas industries use high-strength low-alloy steels (HSLA). The current work focuses on the corrosion of a HSLA steel in the presence of a biphasic environment, in which the oil phase consists of crude oil. The effect of the concentration of naphthenic acids is measured by adding controlled amounts of these acids. The arrangement is meant to mimic the corrosion in tanks of petrochemical plants. The study deals with the use of electrochemical techniques, namely EIS, LEIS, and SECM, with the aim to learn about the applicability of these advanced techniques on the characterization of corrosion in the oil-water complex environments and to give a contribution to the understanding of NAC mechanisms.

2. Experimental

2.1. Materials

The material studied is API 5L X70 steel, whose composition is presented in Table 1.

The crude oil was obtained from an offshore Brazilian pre-salt well, to which naphthenic acids (by Sigma-Aldrich) were added in controlled amounts (up to 10 vol.%). As aqueous electrolyte, a dilute sulfate solution was chosen, to provide a mild electrolyte and thus enhance the corrosive effect of the naphthenic acids, while still ensuring ionic conduction even in the absence of the acids. The solution consisted of 0.01 M Na_2SO_4 (by Sigma–Aldrich) in deionized water (Millipore, conductivity 1.1 $m\Omega^{-1}$ cm^{-1}). All experiments were carried out at ambient temperature.

Table 1
Elemental composition for API 5L X70 steel (grade PSL 1); values correspond to specified maximum mass fraction,%, [31].

C	Mn	P	S	Nb + V + Ti
0.28	1.40	0.030	0.030	0.15

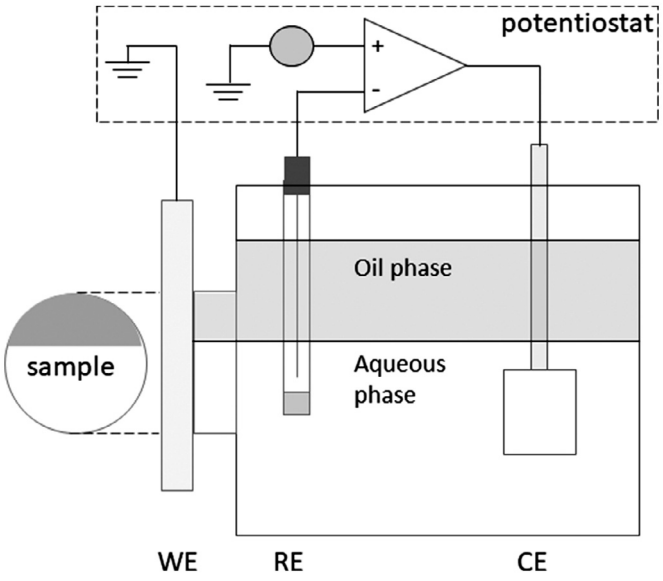

Fig. 1. Experimental scheme for global electrochemical measurements in biphasic - oil and aqueous phases. WE: working electrode, RE: reference, and CE: counter electrode.

2.2. Electrochemical impedance spectroscopy – EIS

For the EIS, the samples consisted of flat plates (3.0 mm thickness). Prior to each experiment, the samples were prepared by abrasion with SiC emery paper up to 1000 mesh, rinsed with Millipore deionized water and ethanol and dried with compressed air. A homemade cell (150 mL volume) was used, in which the sample was exposed vertically and compressed from the outside against an o-ring at a lateral window, leaving an exposed area of 3.14 cm^2. The aqueous solution was poured first and then the oil was added dropwise, preventing contamination of the bottom part of the steel plate, while leaving the metal exposed to both phases – Fig. 1. A platinum wire counter electrode and a commercial Ag|AgCl|KCl (saturated) reference electrode, both immersed in the aqueous phase, completed the setup. Measurements were performed using a PC4 potentiostat coupled to a FAS1 Femtostat (both by Gamry Instruments, PA, USA), in the frequency range 10 kHz – 5 mHz, with 10 mV rms amplitude.

Measurements were made after 60 minutes stabilization at the open circuit potential. The requirement of steady state was ensured by getting two identical full spectra, obtained sequentially. The impedance presented is normalized to the total surface area exposed (3.14 cm^2). In one set of experiments, the area fraction exposed to the aqueous phase, X_{aq}, was varied with the values of 0.05, 0.50, and 0.95, with no addition of naphthenic acids. A sam-

ple exposed to the dilute sulfate solution only (control sample) was also tested. In another set of experiments, naphthenic acids (Sigma-Aldrich) were added to the oil, in concentrations of 1.0, 5.0, and 10 vol.% while the ratio of areas was kept at $X_{aq} = 0.50$ (1:1 area ratio).

Fitting of the impedance spectra was made using Zview software (Scribner Associates), describing the imaginary component of the spectra by a constant phase element (CPE) given by Eq. (1). The parameters Q_o, α, and ω are, respectively the CPE constant and exponent, and the angular frequency.

$$Z_{CPE} = \frac{1}{Q_0(j\omega)^{\alpha}} \quad (1)$$

The capacitance was calculated from the CPE, taking Eq. (2). [32], where R_{ct} is the charge-transfer resistance.

$$C_{dl} = \frac{(Q_o R_{ct})^{\frac{1}{\alpha}}}{R_{ct}} \quad (2)$$

For the inspection and analysis of the surface, exposure was made for 20 h, after which the surface was rinsed with running water, degreased with ethanol, and dried with compressed air. Fourier transform infrared (FTIR) spectroscopy was performed using a Nicolet 5700 spectrometer, equipped with attenuated total reflectance (ATR), with 256 scans and 4.0 cm^{-1} resolution. Inspection of the surface morphology was made by scanning electron microscopy (SEM), using a FEG-SEM/JEOL 7001F system at 20 kV beam energy.

2.3. Localized electrochemical measurements

The surface-resolved techniques were employed to study the local electrochemical activity of the samples, following exposure to the biphasic medium. Resin-embedded samples ($\sim 3.5 \times 20$ mm exposed area) were polished (2400 mesh) and exposed to the biphasic medium for 20 h; subsequently they were rinsed with water and ethanol, dried and finally placed horizontally at the bottom of the cell, containing Na_2SO_4 0.01 M solution, for the localized measurements. For both the LEIS and the SECM techniques, the setup was based upon the M370 Electrochemical Workstation (Uniscan Instruments, U.K.). The sample was inserted from the bottom in a 140 mm diameter electrochemical cell (from Uniscan) and aligned horizontally using a spirit bubble level. The electrolyte volume in the cell was 700 mL, and its surface was approximately 10 mm above the sample. A standard laboratory Ag|AgCl reference electrode (Gamry Instruments) was used; to prevent disturbing the solution or any leaking in the close vicinity of the metal sample, the reference electrode was kept at a safe distance (at least 10 mm) from the studied area.

For the LEIS, the sample was controlled by a potentiostat (Solartron 1286) coupled to a frequency response analyzer (Solartron 1250). The scanning microprobe consisted of a disk-ring commercial device (RSP model, Uniscan Instruments, U.K.) to which the tip was modified to produce a microdisk (diameter 170 µm) [33,34,35]. The disk-to-ring distance was approximately 3 mm. The tip was placed very close to the substrate, using the stepper motor, under visual inspection. An a.c. perturbation with 10 mV rms amplitude was applied to the steel electrode, around its open circuit potential. Measurements were made either in the spectral mode (in which the probe was placed in a fixed position and the frequency was scanned at 1 kHz–100 mHz) or at a fixed frequency (1.0 Hz) and along a horizontal line scan, with step of 160 μm and scan rate 200 μm s^{-1}. A platinum mesh counter electrode and the Ag|AgCl reference electrode completed the cell. The estimated sampled area in each point is around 1.0 mm^2 [33].

The SECM technique was employed for characterizing the local electrochemical activity after exposure of the steel to the biphasic medium. The measurements were made in the dilute aqueous Na_2SO_4, using either the *competition mode* or the *feedback mode*. The competition mode was used to monitor the oxygen depletion near the surface [26,36]. Under diffusion rate control, the current at the tip, i_{lim}, is proportional to the concentration of the reactant, c (Eq. (3)).

$$i_{lim} = 4\ nF\ D\ c\ a \quad (3)$$

With n being the number of electrons transferred in the reaction, D, the diffusivity, a, the tip radius, and F, Faraday's constant. When the scan is made at a short distance from a surface, and provided the oxygen is the only species being reduced at the probe, the regions of the sample with more intense cathodic activity will give a lower cathodic current at the tip. The current was measured with the tip potentiostatically polarized to a potential at which oxygen reduction occurs under diffusion control as (Eq. (4)

$$O_2 + 2H_2O + 4e^- \rightarrow 4OH^-. \quad (4)$$

In the feedback mode, 5.0 mM potassium ferrocyanide was added as mediator, to the 0.010 M Na_2SO_4 electrolyte, and the tip potential was set an anodic value, to force the oxidation at the tip (Eq. (5)):

$$Fe(CN)_6^{4-} \leftrightarrow Fe(CN)_6^{3-} + e^- \quad (5)$$

Depending on the potential and conductivity of the substrate, the mediator may undergo regeneration, which will affect the limiting current measured at the tip. If the mediator undergoes reduction at the surface, then the oxidation current at the tip will increase when it enters the diffusion layer near the surface (positive feedback) while blocking surfaces result in negative feedback.

The SECM was based on a commercial probe (from Sensolytics) consisting of a microelectrode platinum wire (purity 99.99%), sealed and pulled in a quartz glass body, with the active electrode diameter of 10 μm and RG-value >10. The setup was completed with a platinum mesh counter electrode and an Ag|AgCl reference electrode. The operating tip-sample distance was set after recording z-approach curves above the resin and approaching the surface of the resin until the current dropped to 30% of the bulk current. That level was taken as approximately 10 μm height above the surface. Subsequently, the tip was withdrawn to the desired distance. In the results presented, the approach curves were made in the z direction, at 5 μm step size and 5 µm s^{-1}, with a tip potential of E_t= +0.4 V, to force the oxidation of the mediator; the voltammogram is presented as Supplementary Data.

The line scans were made horizontally, at a tip-substrate distance of 20 μm, with a step of 100 μm and 100 μm s^{-1} scan rate, and a tip potential of −0.7 V to monitor the oxygen depletion under limiting diffusion control [29]. At this potential, further to the oxygen reduction reaction (ORR), Fe^{2+} might also become reduced; however, its concentration is negligible, and there were no signs of metal crystallization at the tip. This method allows assessing oxygen depletion with spatial resolution and has its use has been reported for galvanic corrosion [27,37].

3. Results

3.1. Global electrochemical measurements

The effect of the volume fraction of sulfate solution was assessed in a set of spectra having different ratios of aqueous phase/oil phase. Except for the control sample, all the samples had a supernatant oil phase.

The impedance spectrum presents a single capacitive loop – Fig. 2(a) – with the ohmic resistance roughly decreasing with the area of the aqueous phase volume, despite some dispersion, explained by the differences in the positioning of the counter electrode. To ease the comparison, the spectra are also presented

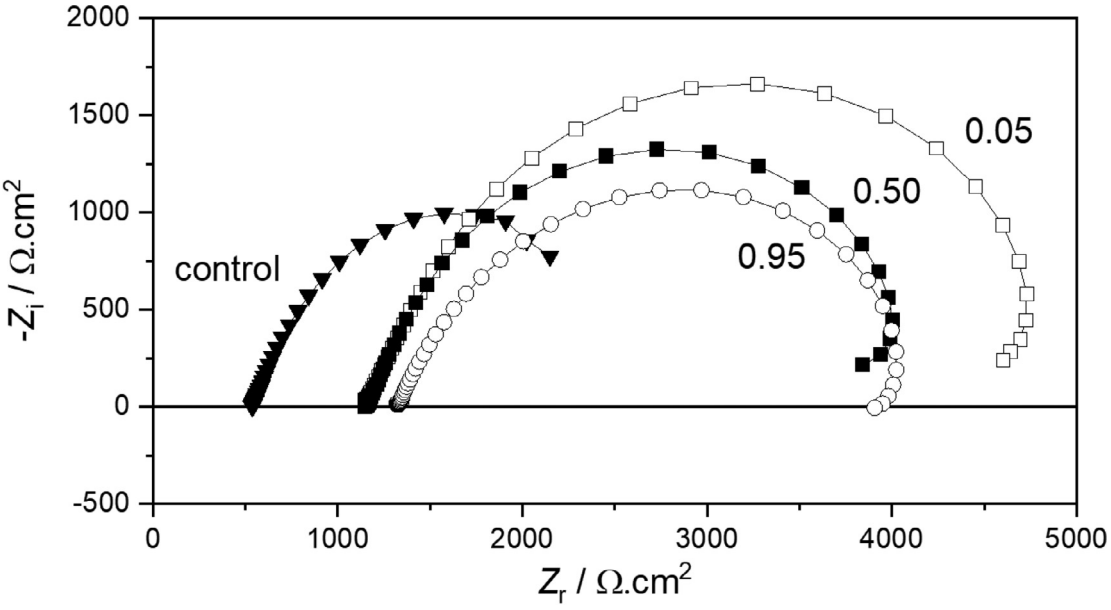

(a)

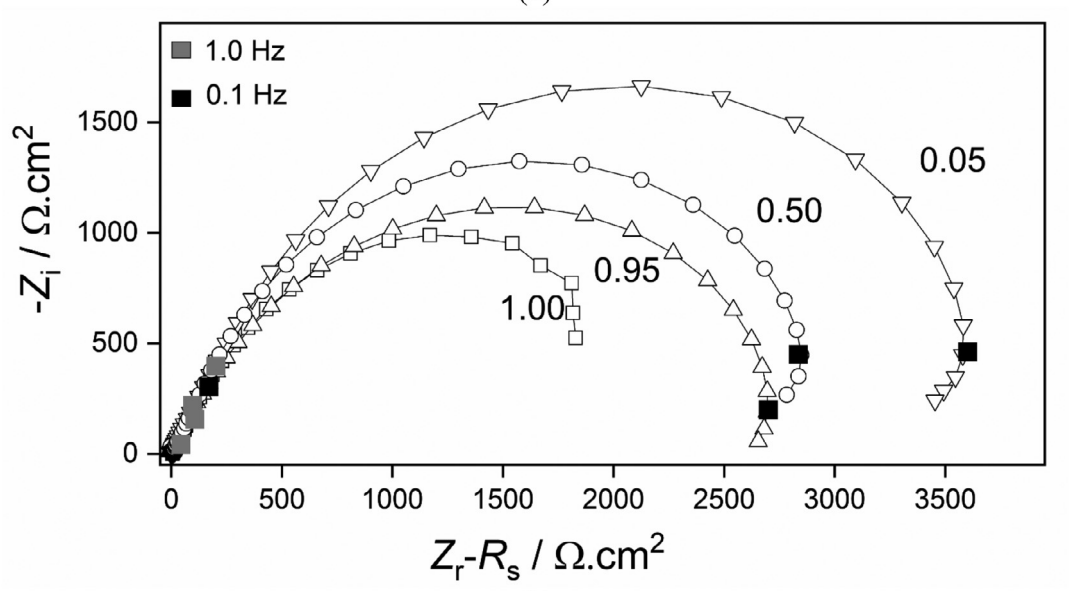

(b)

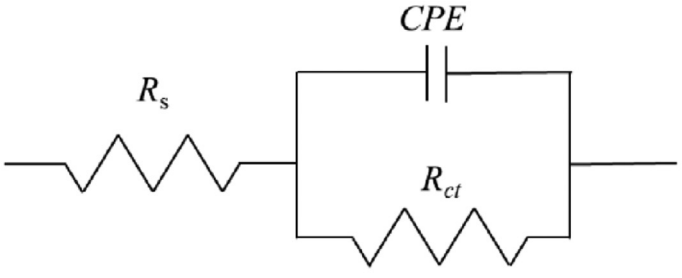

(c)

Fig. 2. EIS spectra of API 5L X70 steel immersed in crude oil/ 0.01 M Na_2SO_4 biphasic medium, for various area fractions exposed to the solution, X_{aq}, as indicated in the plot. Spectra prior to resistance correction (a) and after subtraction of the ohmic resistance (b); The corresponding equivalent electric circuit is presented in (c). Oil was used as received. Impedance is normalized to the total sample area.

Table 2
Parameters from fitting of the spectra (normalized to the overall surface area) and open circuit potential.

X_{aq}	Q_o / Ω^{-1} cm^{-2} s$^{\alpha}$	α	C_{dl} / mF cm^{-2}	R_{ct} / kΩ cm^2	$\tau = R_{ct}.C_{dl}$ / s	E_{ocp} / V (Ag|AgCl)
0.05	2.96×10^{-4}	0.83	0.31	4.1	1.3	−0.65
0.50	3.97×10^{-4}	0.84	0.42	3.2	1.3	−0.64
0.95	1.64×10^{-4}	0.81	0.14	2.9	0.4	−0.67
1.00	2.3×10^{-3}	0.79	3.8	2.8	10	−0.62

after subtraction of the series resistance - Fig. 2(b). The low-frequency region presents a pseudo-inductive tail in the first quadrant, which roughly corresponds to a negative resistance; its origin is not clear, and therefore it is excluded from our interpretation. A simple equivalent circuit was used, comprising a series resistance (R_s) followed by a capacitive component, described as a constant phase element (CPE), and a parallel charge-transfer resistance (R_{ct}) – Fig. 2(c). The charge-transfer resistance grows with the decreasing fraction of the aqueous phase. It is in the range 2000 – 4000 Ω cm^2, a value that is higher than the 100 – 700 Ω cm^2 reported for exposure to oil/water emulsions impingement corrosion [16]. It is much lower than the 10^8– 10^9Ω cm^2 parallel resistance reported by Perini et al. [17] for oil; further, our results consist of a single semi-circle, while those authors assigned a high-frequency semi-circle to the oil (continuous phase) and a lower frequency semi-circle to the emulsion [17]. Since we do not have a continuous and dispersed phase, but rather two phases in parallel, the results are consistent with the impedance being due to the electrochemical activity at aqueous interface only, resulting from the high ohmic resistance of the oil [16].

The exponent α is approximately 0.8 in all samples, with minor variations, while the Q_o and the capacitance are consistent with a double layer. Unlike the capacitance and the resistance, the time constant (τ) does not depend on the area. Its value is in the range 1 – 10 seconds (Table 2). This is far too high for the oil phase, for which around 10 ms was reported [17] and we thus assign it to the processes at the metal/water phase interface. The charge transfer resistance decreases with the fraction of area exposed to the aqueous phase, X_{aq} – Fig. 3(a) and Table 2. Assuming that the electrochemical activity measured comes from the aqueous phase only, accounting for the overall area likely means that the apparent resistance is overestimated. When only the fraction of aqueous area is accounted for – Fig. 3(b) – the opposite trend is observed, *i.e.*, the charge transfer resistance increases as the aqueous phase becomes predominating.

The open circuit potential was in the range −600 to −680 mV; it gradually decreased in the sample exposed to the sulfate solution only due to depletion of oxygen, while it was quite stable from the start of immersion in the samples in the biphasic medium (Supplementary Data). Further, d.c. polarization (Supplementary Data) shows that the cathodic reaction is controlled by diffusion in the simple immersion in the sulfate solution (meaning that oxygen reduction is the cathodic process), while under an oil layer, the open circuit potential becomes slightly more negative and the reaction is activation-controlled, *i.e.*, water is the cathodic reactant. These results show a difference in the cathodic reaction, which is that of oxygen in normal aqueous exposure, while water becomes the cathodic reactant in the presence of the upper oil layer, thus altering the corrosion mechanism.

The spectra in Fig. 4 depict the effect of the naphthenic acid on the electrochemical activity of the system. Addition of 1% and 5% of HNap caused an evident decrease of the size of the impedance arc, while adding up to 10% caused no further effect. The charge-transfer resistance obtained through fitting gives a consistent evolution, stabilizing at approximately 1.6 kΩ cm^2– Fig. 5. The evolution suggests dissociation of the HNap in the aqueous phase [38], making the electrolyte more aggressive and thus increasing the

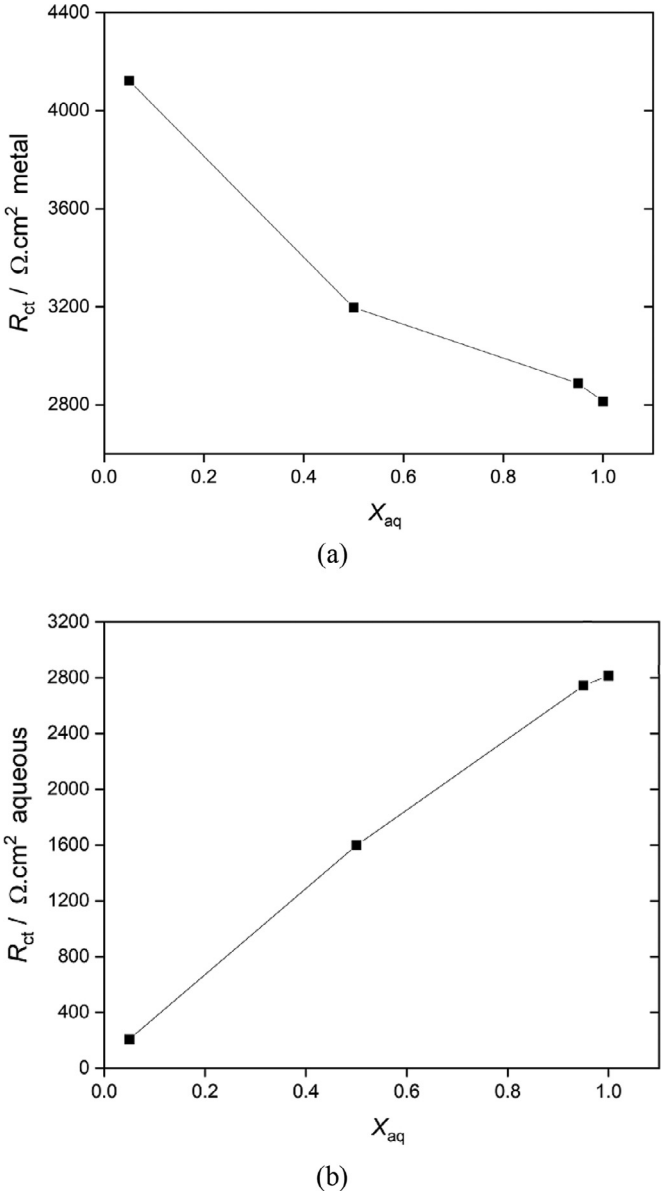

Fig. 3. Charge-transfer resistance of API 5L X70 steel immersed in crude oil/ 0.01 M Na_2SO_4 biphasic medium for various area fractions exposed to the aqueous phase: values obtained from the spectra in Fig. 2, normalized to the overall area (a) or to the area of the metal/aqueous phase only (b).

electrochemical activity at the surface. This is supported by the pH measurements made in the aqueous phase before and after the experiment, which has revealed a pH drop from 6.0 to 4.5 (in the system with addition of 5% HNap), after 1 h of contact.

3.2. Surface inspection and analysis

Following immersion, the samples revealed a spatial distribution of corrosion attack and morphology. The regions exposed to

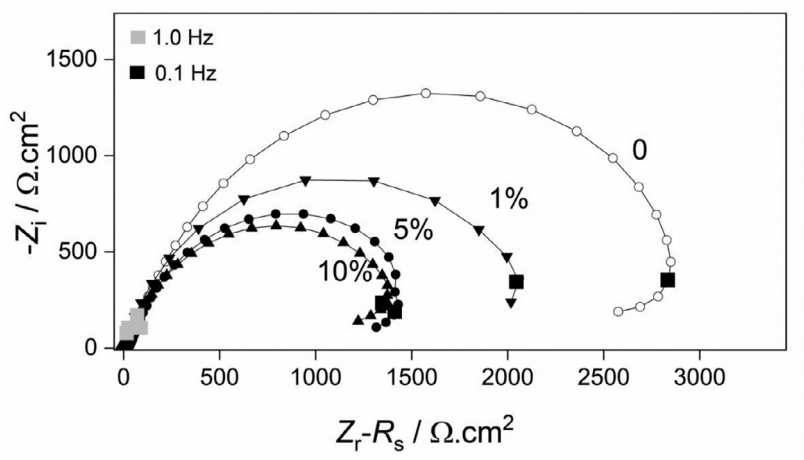

Fig. 4. Impedance spectra of API 5L X70 steel exposed to crude oil/ 0.01 M Na_2SO_4 biphasic medium, for varying naphthenic acid content in the oil phase, with $X_{aq} = 0.50$. Spectra are normalized to the overall area, and the series resistance was subtracted.

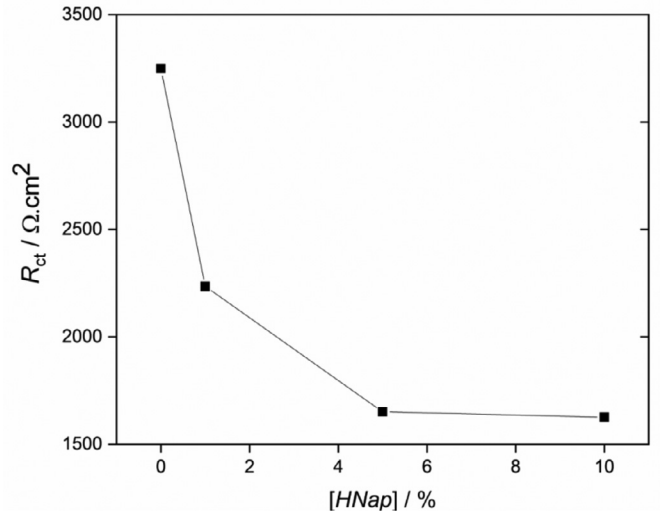

Fig. 5. Effect of the naphthenic acid content on the charge transfer resistance of API 5L X70 steel exposed to crude oil/ 0.01 M Na_2SO_4 biphasic medium, measured by EIS. $X_{aq} = 0.50$; values obtained from the spectra in Fig 4 and normalized to the overall area.

the oil phase show no signs of corrosion (Fig. 6(a)), while severe and extensive attack was observed just below the interface (Fig. 6(b,c)), in the aqueous region. On this region of the surface the attack was uniform, leading to a rough surface and no distinction among pits. Finally, deeper and further away from the oil phase, a few millimeters below the oil, the attack became gradually more localized, as isolated crater-shaped pits - Fig. 6(d).

The spatial distribution and morphology of the anodic dissolution reveals localized attack, with the anodic reaction occurring at the water phase, but mostly restricted to a small area near the oil. This could be due either to an increased acid concentration near the oil phase, as it diffuses from the oil, or to a spatial separation between the cathodic and the anodic reactions. This second explanation, based upon a higher solubility of oxygen in oil and the formation of a galvanic process between the oil and the aqueous phase, has been discussed by Becerra et al. [16]; while it seems reasonable in industrial conditions, due to the thin oil layers in a moving emulsion, it is hard to accept in stagnant conditions, under a relatively thick layer of oil. The most likely cause for the localized corrosion is therefore the higher concentration of HNap in the upper aqueous region, close to the oil, consequence of the slow diffusion and the partition coefficient of the carboxylic acids, with the acceleration of both the anodic and the cathodic reactions [39].

When the steel was exposed to dry oil, *i.e.*, with no water, the FTIR spectrum revealed a clean surface (Fig. 7, curve (a)), with no sign of corrosion products or even of the naphthenic acid, while exposure to the dilute sulfate seems to generate lepidocrocite (γ–FeOOH) (curve (d)), identified by the bands at 1018 cm^{-1} (in-plane vibration) and 750 cm^{-1} (out-of-plane vibration) [40,41]. These bands are also observed in the samples corroded in the biphasic medium (curves (b) and (c)), together with the broad band centered at 3250 – 3300 cm^{-1}, assigned to O–H stretching, likely due to iron hydroxides. Although the formation of lepidocrocite is not expected with an open circuit potential below −0.6 V or with unaerated water, because oxygen or some other strong oxidant is required for the conversion to Fe(III), it may however result from some oxidation of ferrous compounds in air, after removal from the solution. On the other hand, curves (b) and (c) show no signs of carboxylic acid, which would require a characteristic peak of C=O, at 1720 cm^{-1} [42]; instead, carboxylates (*i.e.*, the naphthenates) are revealed [43] by the bands at 1655 and 1414 cm^{-1}, both above and below the interface. The similarity of the surface in the two regions does not match the contrast observed in the SEM inspection, but it rather suggests that the naphthenate, formed only in the presence of the aqueous phase, may diffuse into the oil phase where it precipitates on the surface.

3.3. Local electrochemical measurements

In the post-exposure study, the region pre-exposed to the oil phase became more reactive, as revealed by a drop of the overall impedance by approximately one order of magnitude – Fig. 8. Although the results should be interpreted in a qualitative way, the effective area of the aqueous region is much higher, which might justify a lower impedance. However, the oil region has a higher admittance, by around one order of magnitude in relation to aqueous region. This could mean that either this region became protected by the oil during the exposure, or the aqueous region became protected by some iron oxides following the exposure.

The impedance scan lines confirm the lower impedance on the side pre-exposed to the oil – Fig. 9. Further, the impedance consistently decreased as the probe approached the surface. This was more consistent on the side of the non-corroded surface, while on the corroded side (exposed to the aqueous phase) the distance of the probe to the surface had a just a minor effect. The line scans were made at various heights because the dissolution of mate-

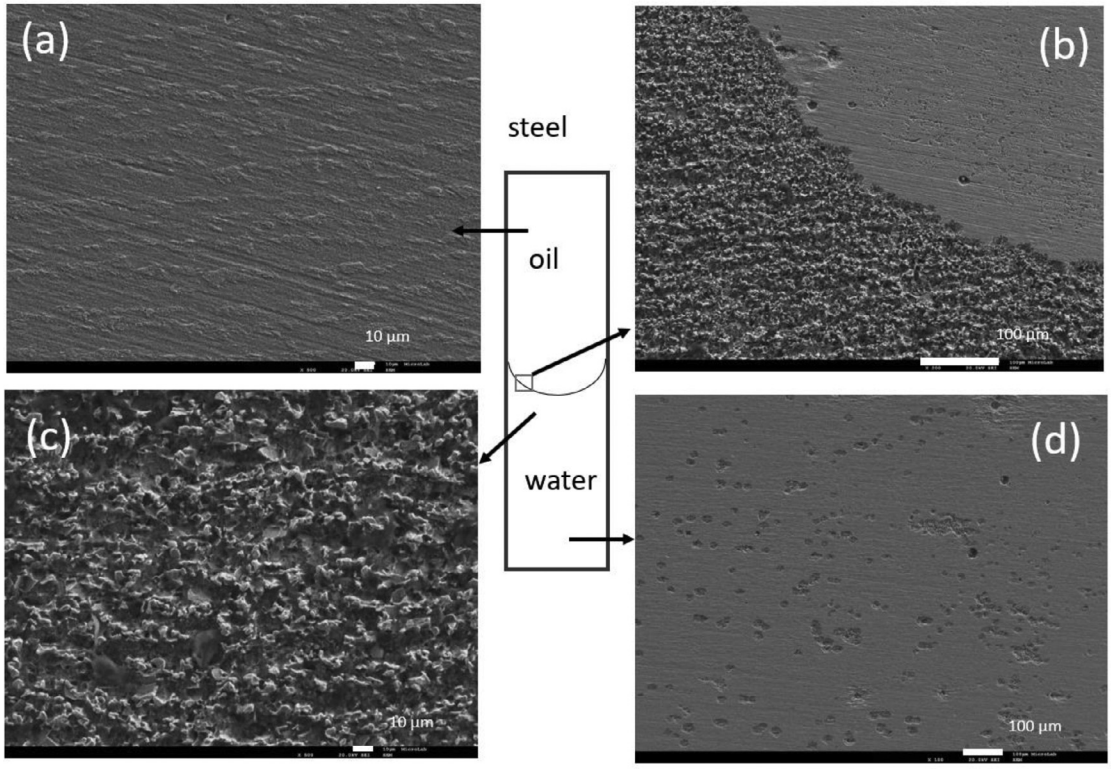

Fig. 6. SEM micrographs of API 5L X70 steel after exposure to crude oil + 5% HNap / 0.01 M Na_2SO_4 biphasic medium, at the oil region (a), at the interface (b), just below the interface (c), and in the aqueous region at a distance from the oil (d).

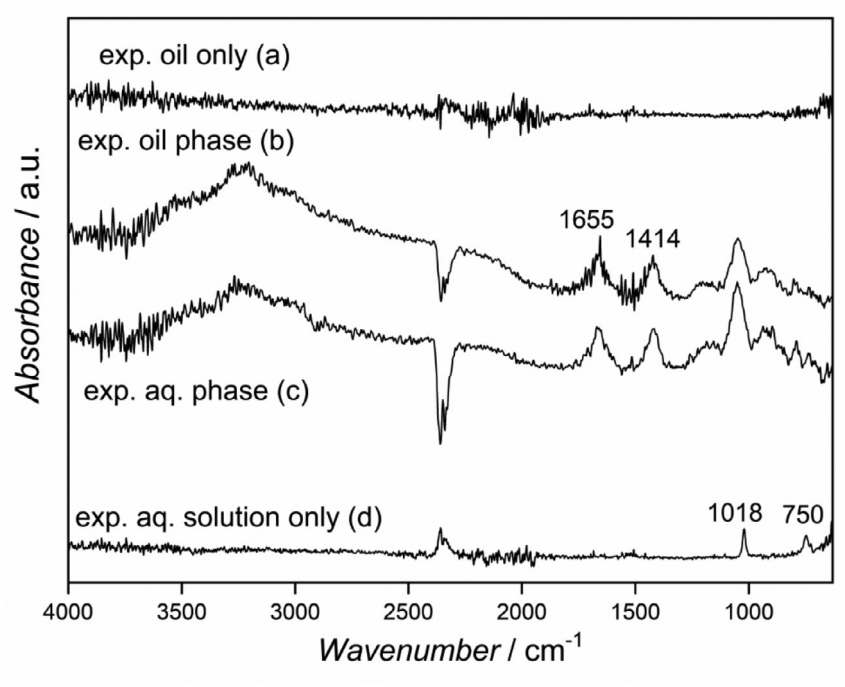

Fig. 7. FTIR spectra of API 5L X70 steel surface after exposure to the as-received crude oil (a); the oil phase, in the oil + 5% HNap/0.01 M Na_2SO_4 biphasic system (b); the aqueous phase in the same biphasic system, at the region just below the interface (c); the Na_2SO_4 0.01 M solution only (d).

rial may increase the tip-sample distance. However, the average local impedance difference between the two sides is well above the difference caused by the probe height (as confirmed by the curves obtained at 20 and 220 μm height, z). Hence, the profile cannot be ascribed to any roughness effect caused by corrosion but rather results from the differences in electrochemical reactivity. As the probe moves to the corroded region (pre-exposed to the aqueous phase), the impedance rises, likely due to the accumulation of corrosion products. Unlike the oil-exposed area, a plateau is never reached; this impedance profile is likely due to the contribution of the more active neighboring region on the left of the diagram.

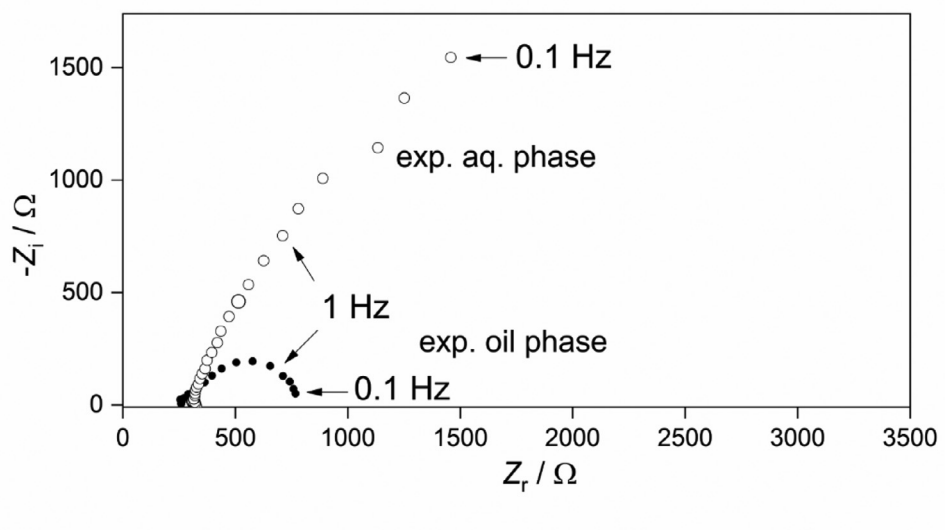

Fig. 8. Local impedance spectra of API 5L X70 steel in Na_2SO_4 0.01 M Sample pre-exposed for 20 h to the oil/0.01 M Na_2SO_4 biphasic system.

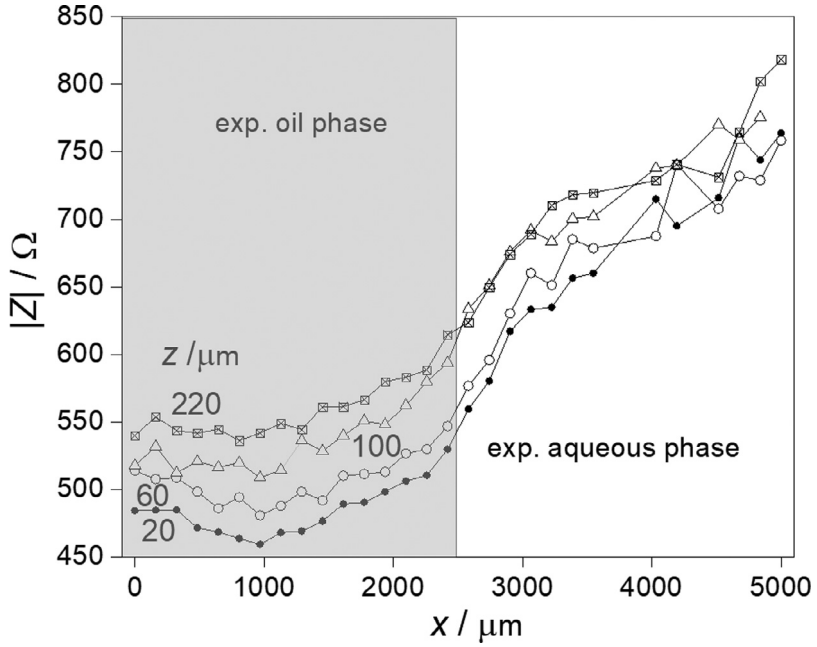

Fig. 9. Impedance modulus at 1.0 Hz, measured in Na_2SO_4 0.01 M, along API 5L X70 steel surface, pre-exposed to the oil/0.01 M Na_2SO_4 biphasic system, for different heights *z* above the metallic surface.

The tip current measured in the SECM experiments revealed a tendency for contamination during continued experiments, which resulted in low measured currents. Still, the approach curves revealed positive feedback currents, meaning that the metal is electroactive in both regions. This feedback current is higher on the region previously exposed to the oil, *i.e.*, which gained a higher regeneration capacity (Fig. 10). This means that the surface was cleaner from any insulating films, compared to the region exposed to the aqueous phase. The highest tip current, measured at the surface, is approximately 0.195 nA in the aqueous region, vs. 0.29 nA in the oil region. This has no direct correlation with the corrosion rate, but it rather reveals a surface that regenerates the mediator at a faster rate, thus being more capable of transferring electrons at the surface.

The line-scans obtained across the metal with $E_t = -0.70$ V reveal lower currents locally, compared to the mounting resin – Fig. 11. Over the inert resin the reduction current is approximately 0.6 to 0.8 nA, with some lateral asymmetry resulting from the probe movement, that can push some fluid during the scan. The decreased cathodic current measured locally reveals depletion of oxygen, and thus cathodic activity, near the substrate [30]. The depletion is more significant in the steel pre-exposed to oil, likely due to the absence of corrosion products.

4. Discussion

The oil has a very low ionic conductivity, of approximately 0.486 μSm^{-1}[17], six orders of magnitude below that of the diluted aqueous Na_2SO_4 (estimated as ~0.24 Sm^{-1}[39]), therefore the two phases in parallel result in the measurement coming mostly from the more conductive of the two phases. The consistent variation of impedance with the water/oil ratio, as well as the high time constant of the electrochemical process, support the interpretation that the electrochemical response measured is due to the aqueous

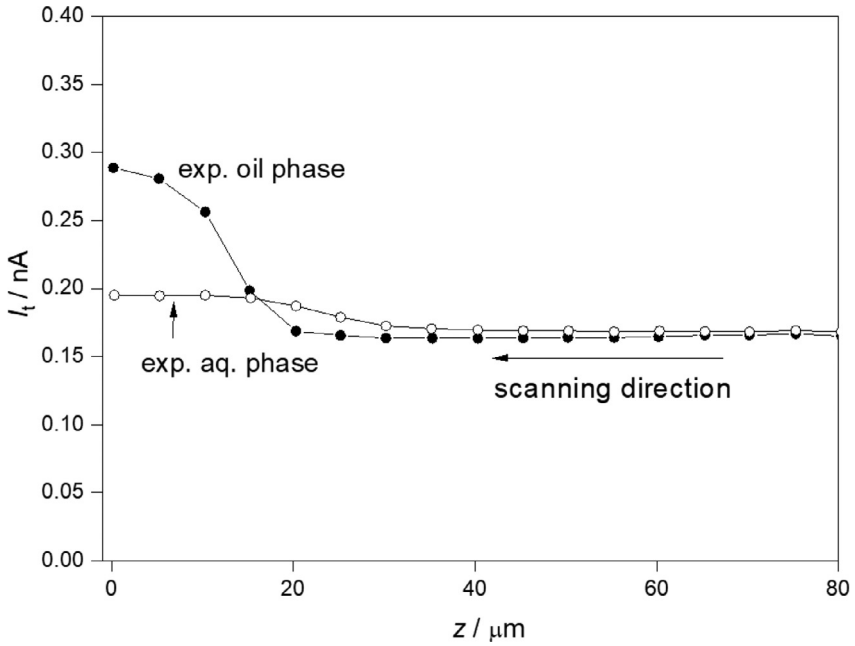

Fig. 10. SECM amperometric approach currents measured in $K_4[Fe(CN)_6]$ + Na_2SO_4 0.01 M, with tip potential, E_t = 0.4 V. Position z = 0 corresponds to the API 5L X70 steel surface, pre-exposed to the crude oil + 5% HNap/0.01 M Na_2SO_4 biphasic medium.

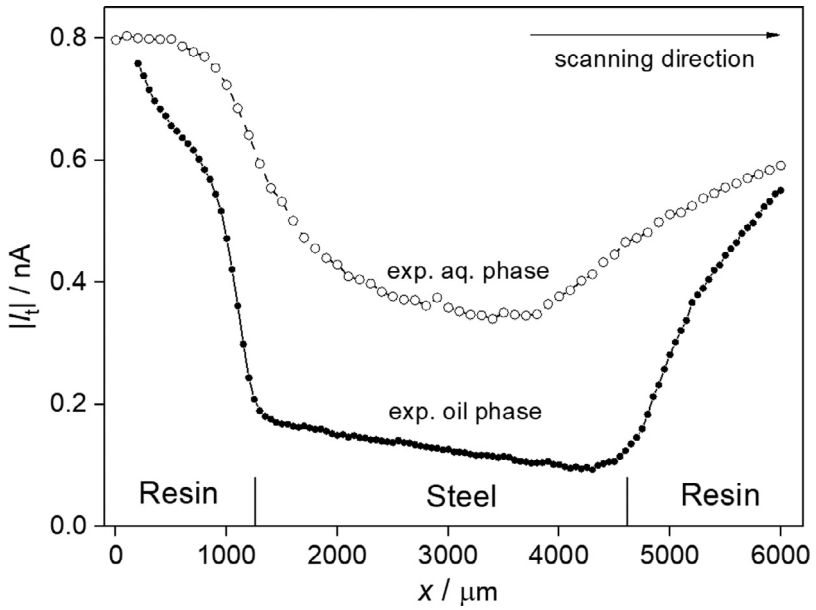

Fig. 11. SECM amperometric horizontal line-scans in 0.01 M Na_2SO_4 solution, at E_t = −0.7 V; sample consists of API 5L X70 steel, pre-exposed to crude oil + 5% HNap/0.01 M Na_2SO_4.

phase. The apparent decrease of the charge transfer resistance with the water content seems to agree with the observations reported in crude oil/brine mixtures [42], in which the amount of crude oil seemed to lower the corrosion rate of the steel products. However, once the oil phase is excluded from the active area normalization, we observe the opposite trend, *i.e.*, the charge-transfer resistance increases with the area fraction of the aqueous phase, meaning that the corrosion rate effectively increases with the oil amount. While Efird and Jasinski [42] interpreted the apparent protection of the oil based upon the effect of the corrosion products, we conclude that the difference results essentially from the lack of identification of the two phases i.e., from the determination of the effective area of each phase.

Electrochemical measurements dealing with oil corrosion are commonly performed in model emulsions [42], in which kerosene is often used as the oil component while the reference electrode is usually inserted via a Luggin capillary, which lowers the junction potential, while preventing contamination of the reference half-cell. While contamination of the reference electrode can lead to disturbed potential readings [44], the use of an emulsified electrolyte leads to uniform dissolution, masking mechanistic and spatial effects. The approach used in this work, while preventing contamination of the electrodes, evidences the effect of the naphthenic acid, while still allowing the contact between the two phases and the metal surface. This is a better alternative to the use of aqueous extracts from the oil, in which the acid be-

comes uniformly dissolved, while the spatial distribution of corrosion misses the proximity of the oil phase, source of the naphthenic acids. Moreover, the use of diluted sodium sulfate solution instead of the more common sodium chloride, essentially restricts the corrosive effects to the effect of the naphthenic acids. Finally, the oil layer blocks the contact with air, hindering the diffusion of oxygen down to the metal surface. The arrangement used thus has several advantages, despite its deviation from service conditions that can occur under turbulent regime.

Acids in crude oil dissolve to some degree into the water phase or adsorb at the oil/water interface, depending on the pH, molecular structure, and molecular size [45]. In the oil phase, the naphthenic acids become stabilized by forming dimers, in which the carboxylic terminal becomes coupled, while at interfaces they become stabilized by self-assembling, with the non-polar part (cyclopentyl or cyclohexyl rings) in the organic phase and the carboxyl terminal, in the aqueous phase [46]. They present partition into the water phase by proton donation, i.e., ionization. The proton combines with hydroxyl ion (OH^-) at sufficiently high pH, while the negatively charged Nap^- becomes partitioned into the water. The partition coefficient varies linearly with the number of carbon atoms in the acid hydrocarbon chain and determines the critical pH, i.e., the pH at which the fraction of ionized acid at the interface exceeds 0.5 [46]. Naphthenic acids have a variable number of carbon atoms in the range C10-C30 [47,48]. For C14 naphthenic acids with one or two rings, partition coefficients are reportedly around 10^{-5}, while smaller molecules may reach partition coefficients two orders of magnitude higher [39,46], thus more readily dissolving in the aqueous phase. For molecular weight 209–233 g/mol, some partition into the water phase has been observed starting above pH~5 [49], while concentrations as high as 100 mg/L after prolonged natural contact of water have been reported, even at low temperature [50].

According to the mechanism proposed for high-temperature NAC [51], the first step is the acid dissociation at the interface (Eq. (6)):

$$(R[CH_2]_nCOOH)_{2oil} \rightarrow 2R[CH_2]_nCOO^-_{aq} + 2H^+. \quad (6)$$

In water, the ionized molecule likely becomes stabilized through the formation of micelles, with the organic chain at the core of the micelle structure and the polar carboxyl terminal in the outer region. The formation of micelles of the acids requires a critical concentration [52], therefore its formation must be restricted to the region near the interface, where the concentration is maximal. The cathodic reaction is the hydrogen evolution reaction (Eq. (7), while the oxidized iron ions become complexed by the carboxylate – reactions, (Eqs. (8)–(10)) [50].

$$H^+ + 2e^- \rightarrow H_2 \quad (7)$$

$$Fe \rightarrow Fe^{2+} + 2e^- \quad (8)$$

$$Fe^{2+} + 2R[CH_2]_nCOO^- \rightarrow Fe[R[CH_2]_nCOO]_2 \quad (9)$$

Finally, part of the iron naphthenates diffuse into the oil phase, where they become adsorbed on the surface:

$$Fe[R[CH_2]_2COO]_2 \rightarrow Fe[R[CH_2]_nCOO]_{2,\,oil} \quad (10)$$

The major difference in our observations lies in the relevance of the diffusion of the naphthenic acids in the water phase, resulting in intense corrosion at a thin region near the interface.

The corrosion morphology, of crater-shaped pits in the early corrosion stages, reveals some form of pseudo-passivity, due either to an oxide layer or to the adsorption of organic species [46]. The pits do not grow in depth, but rather tend to coalesce, evolving towards an apparently uniform attack. There are reports that naphthenic acids favor uniform corrosion compared to pitting attack in sulfiding solutions (with H_2S) [13,19]. However, we observe that corrosion rather starts as a localized attack, then extending towards a uniform process.

The localized electrochemical techniques, used after the exposure in the aqueous/oil system, can be considered as an *ex-situ* study, although performed in immersion. Its purpose is to compare the state of the surface with respect to the activity and possible film formation. The comparative lower impedance, together with the more significant depletion of oxygen and the higher feedback current of the region previously exposed to oil, reveals a more active surface when left in the aqueous solution and with access to oxygen. The presence of naphthenate, likely resulting from adsorption onto the steel surface [13], does not produce corrosion locally but likely activates the surface upon the new immersion in aqueous phase only. The reason for this difference was not explored, although it may be due either to the simple solubilization of the naphthenate when in contact with water, or to some electrochemical conversion of the naphthenates themselves.

The setup used in surface-resolved techniques is limited by the horizontal scanning, which excludes the use of a biphasic medium, but it is also limited by the risk of contamination of the probes; nevertheless, the protocol used has given results quite comparable with those obtained on bare metals or galvanic systems [30]. The study, although not extensive, shows a marked difference between the two regions of the steel surface. These results open new chances for the use of advanced techniques on more technical and complex systems.

5. Conclusions

The morphology of naphthenic acid corrosion of steel in a stagnant biphasic medium consisting of crude oil and water, with no emulsification, can be described by three regions: (a) up in the oil phase, the steel surface is immune to corrosion; (b) in the aqueous phase, in the vicinity of the oil, severe uniform corrosion occurs; (c) deep in the water phase, at a distance from the oil, slight corrosion occurs as crater-shape pits scattered along the otherwise intact surface.

Increasing concentrations of naphthenic acids in the crude oil, increased the corrosion rate in the aqueous region. Once only the area exposed to the aqueous phase is considered, for stagnant condition and in the absence of water/oil emulsion, the corrosion rate increases with the oil fraction, even though corrosion is restricted to the water phase.

The experimental arrangement using a stagnant biphasic medium allows corrosion monitoring using electrochemical techniques and provides information involving spatial distribution of the corrosion processes. Electrochemical impedance spectroscopy measurement across the aqueous phase only, while keeping part of the electrode exposed to an oil phase, allows to monitor the indirect effect of the oil phase. The setup used reveals information of specific field conditions, in which phase separation influences the morphology and mechanism of corrosion.

The localized electrochemical techniques reveal that, once removed from the biphasic medium, the area exposed to the oil has comparatively lower impedance, higher cathodic activity for the reduction of oxygen and a higher feedback current for regeneration of the potassium ferrocyanide mediator in SECM measurements.

A model for the naphthenic acid corrosion of steel at ambient temperature is proposed, based upon the partial solubilization of the naphthenic acids in the aqueous phase and complexation of ferrous ions in the water phase. Corrosion is restricted to the water phase, although influenced by the concentration of acid in the oil. The resulting iron naphthenate may partially dissolve back into the oil phase and precipitate on the surface.

Funding

This research had the financial support of the Brazilian agencies R.M.P.S. (Fapesp 2013/19903–0 and 2017/10526–0), H.B.S. (CNPq 305455/2014–1, Fapesp 2014/13601–2), I.N.B. (Capes - Finance Codes 001 and 88881–118836/2016–01), and the Portuguese Fundação para a Ciência e Tecnologia, FCT (UIDB/00100/2020 and UIDP/00100/2020).

Declaration of Competing Interest

The authors declare no conflict of interest. The funders had no role in the design of the study; in the collection, analyses, or interpretation of data; in the writing of the manuscript, or in the decision to publish the results.

Supplementary materials

Supplementary material associated with this article can be found, in the online version, at doi:10.1016/j.electacta.2022.139900.

Credit authorship contribution statement

Rejane M.P. Silva: Conceptualization, Methodology, Investigation, Writing – original draft, Writing – review & editing. **Hugo B. Suffredini:** Conceptualization, Project administration. **Ivan N. Bastos:** Methodology, Investigation, Writing – original draft, Writing – review & editing. **Luis F. Santos:** Formal analysis, Writing – review & editing. **Alda M.P. Simões:** Conceptualization, Resources, Writing – review & editing.

References

[1] S. Nešić, Key issues related to modelling of internal corrosion of oil and gas pipelines-a review, Corros. Sci. 49 (2007) 4308–4338, doi:10.1016/j.corsci.2007.06.006.
[2] E. Slavcheva, B. Shone, A. Turnbull, Review of naphthenic acid corrosion in oil refining, Br. Corros. J. 34 (1999) 125–131, doi:10.1179/000705999101500761.
[3] D. Qu, Y. Zheng, X. Jiang, W. Ke, Correlation between the corrosivity of naphthenic acids and their chemical structures, Anti-Corros. Methods Mater. 54 (2007) 211–218, doi:10.1108/00035590710762348.
[4] H.P. Dias, P.V. Dixini, L.C.P. Almeida, G. Vanini, E.V.R. Castro, G.M.F.V. Aquije, A.O. Gomes, R.R. Moura, V. Lacerda, B.G. Vaz, W. Romão, Evidencing the crude oil corrosion by Raman spectroscopy, atomic force microscopy and electrospray ionization FT-ICR mass spectrometry, Fuel 139 (2015) 328–336, doi:10.1016/j.fuel.2014.08.065.
[5] H.P. Dias, E.V. Barros, A.O. Gomes, R.R. Moura, F.E. Pinto, A.S. Gonçalves, G.M.F.V. Aquije, Z. Xu, W. Romão, Corrosion rate studies of AISI 1020 steel using linear, cyclic, and aromatic naphthenic acid standards, J. Pet. Sci. Eng. 184 (2020) 106474, doi:10.1016/j.petrol.2019.106474.
[6] G.M. Bota, D. Qu, S. Nesic, H.Alan Wolf, Naphthenic acid corrosion of mild steel in the presence of sulfide scales formed in crude oil fractions at high temperature, in: Proceedings of the Corrosion 2010 Conference & Expo, NACE International, 2010.
[7] J. Yu, L. Jiang, F. Gan, High temperature naphthenic acid corrosion of steel in high TAN refining media, Anti-Corros. Methods Mater. 55 (2008) 257–263, doi:10.1108/00035590810903845.
[8] D.R. Qu, Y.G. Zheng, H.M. Jing, Z.M. Yao, W. Ke, High temperature naphthenic acid corrosion and sulphidic corrosion of Q235 and 5Cr1/2Mo steels in synthetic refining media, Corros. Sci. 48 (2006) 1960–1985, doi:10.1016/j.corsci.2005.08.016.
[9] P.P. Alvisi, V.F.C. Lins, An overview of naphthenic acid corrosion in a vacuum distillation plant, Eng. Fail. Anal. 18 (2011) 1403–1406, doi:10.1016/j.engfailanal.2011.03.019.
[10] N. Jauseau, S. Nesic, A study of the flow effect on naphthenic acid corrosion of mild steel, in: Proceedings of the Corrosion 2016 Conference & Expo, NACE International, Houston, 2016.
[11] M. Moradi, E. Topchiy, T.E. Lehmann, V. Alvarado, Impact of ionic strength on partitioning of naphthenic acids in water-crude oil systems-determination through high-field NMR spectroscopy, Fuel 112 (2013) 236–248, doi:10.1016/j.fuel.2013.05.024.
[12] A. Bertheussen, S. Simon, J. Sjöblom, Equilibrium partitioning of naphthenic acids and bases and their consequences on interfacial properties, Colloid. Surf. A Physicochem. Eng. Asp. 529 (2017) 45–56, doi:10.1016/j.colsurfa.2017.05.068.
[13] E.C. Rios, A.L. Oliveira, A.M. Zimer, R.G. Freitas, R. Matos, E.C. Pereira, L.H. Mascaro, *In situ* characterization of naphthenic corrosion of API 5L X70 steel at room temperature, Fuel 184 (2016) 648–655, doi:10.1016/j.fuel.2016.07.068.
[14] P. Schütz, É. Castilhos, L.M. Rodrigues, L.F.P. Dick, The influence of inclusions and naphthenic acids on the corrosion of pipeline steels, ECS Trans. 3 (2019) 173–179, doi:10.1149/1.2721441.
[15] F. Hass, A.C.T.G. Abrantes, A.N. Diógenes, H.A. Ponte, Evaluation of naphthenic acidity number and temperature on the corrosion behavior of stainless steels by using electrochemical noise technique, Electrochim. Acta 124 (2014) 206–210, doi:10.1016/j.electacta.2013.08.090.
[16] H.Q. Becerra, C. Retamoso, D.D. Macdonald, The corrosion of carbon steel in oil-in-water emulsions under controlled hydrodynamic conditions, Corros. Sci. 42 (2000) 561–575, doi:10.1016/S0010-938X(99)00068-2.
[17] N. Perini, A.R. Prado, C.M.S. Sad, E.V.R. Castro, M.B.J.G. Freitas, Electrochemical impedance spectroscopy for *in situ* petroleum analysis and water-in-oil emulsion characterization, Fuel 91 (2012) 224–228, doi:10.1016/j.fuel.2011.06.057.
[18] E.B. Zeinalov, V.M. Abbasov, L.I. Alieva, Petroleum acids and corrosion, Pet. Chem. 49 (2009) 185–192, doi:10.1134/S0965544109030013.
[19] E.C. Rios, A.M. Zimer, P.C.D. Mendes, M.B.J. Freitas, E.V.R. de Castro, L.H. Mascaro, E.C. Pereira, Corrosion of AISI 1020 steel in crude oil studied by the electrochemical noise measurements, Fuel 150 (2015) 325–333, doi:10.1016/j.fuel.2015.02.022.
[20] M.G. Mahjani, J. Neshati, H.P. Masiha, M. Jafarian, Electrochemical noise analysis for estimation of corrosion rate of carbon steel in crude oil, Anti-Corros. Methods Mater. 54 (2007) 27–33, doi:10.1108/00035590710717366.
[21] Y. Tan, Experimental methods designed for measuring corrosion in highly resistive and inhomogeneous media, Corros. Sci. 53 (2011) 1145–1155, doi:10.1016/j.corsci.2011.01.018.
[22] L. Goual, Impedance spectroscopy of petroleum fluids at low frequency, Energy Fuels 23 (2009) 2090–2094, doi:10.1021/ef800860x.
[23] V.F. Lvovich, M.F. Smiechowski, Impedance characterization of industrial lubricants, Electrochim. Acta 51 (2006) 1487–1496, doi:10.1016/j.electacta.2005.02.135.
[24] R.M.P. Silva, L.C. Lima, I. Gaubeur, H.B. Suffredini, On the use of dispersive liquid-liquid microextraction combined with organic/water interface electrochemistry, Electroanalysis 29 (2017) 259–263, doi:10.1002/elan.201600429.
[25] R.M.P. Silva, M.C. Maynart, H.B. Suffredini, Ferrocene partition calculation in a biodiesel/water interface using electrochemical methods, Ionics 20 (2014) 1183–1188 (Kiel), doi:10.1007/s11581-014-1116-1.
[26] K.C. Leonard, A.J. Bard, The study of multireactional electrochemical interfaces via a tip generation/substrate collection mode of scanning electrochemical microscopy: the hydrogen evolution reaction for Mn in acidic solution, J. Am. Chem. Soc. 135 (2013) 15890–15896, doi:10.1021/ja407395m.
[27] A.C. Bastos, A.M. Simões, S. González, Y. González-García, R.M. Souto, Imaging concentration profiles of redox-active species in open-circuit corrosion processes with the scanning electrochemical microscope, Electrochem. Commun. 6 (2004) 1212–1215 and Electrochem. Commun. 7 (2005) 1183–1184, 10.1016/j.elecom.2005.07.016 (corrigendum), doi:10.1016/j.elecom.2004.09.022.
[28] A.C. Bastos, A.M. Simões, S. González, Y. González-García, R.M. Souto, Application of the scanning electrochemical microscope to the examination of organic coatings on metallic substrates, Prog. Org. Coat. 53 (2005) 177–182, doi:10.1016/j.porgcoat.2005.02.005.
[29] A.G. Marques, J. Izquierdo, R.M. Souto, A.M. Simões, SECM imaging of the cut edge corrosion of galvanized steel as a function of pH, Electrochim. Acta 153 (2015) 238–245, doi:10.1016/j.electacta.2014.11.192.
[30] M. Mouanga, M. Puiggali, B. Tribollet, V. Vivier, N. Pébère, O. Devos, Galvanic corrosion between zinc and carbon steel investigated by local electrochemical impedance spectroscopy, Electrochim. Acta 88 (2013) 6–14, doi:10.1016/j.electacta.2012.10.002.
[31] Specification for line pipe - API specification 5L, Upstream segment, 45th ed., (December 2012). American Petroleum Institute, Washington DC USA.
[32] G.J. Brug, A.L.G. van Eeden, M. Sluyters-Rehbach, J. Sluyters, The analysis of electrode impedances complicated by the presence of a constant phase element, J. Electroanal. Chem. 176 (1984) 275, doi:10.1016/S0022-0728(84)80324-1.
[33] J.B. Jorcin, E. Aragon, C. Merlatti, N. Pébère, Delaminated areas beneath organic coating: a local electrochemical impedance approach, Corros. Sci. 48 (2006) 1779–1790, doi:10.1016/j.corsci.2005.05.031.
[34] V.M.W. Huang, V. Vivier, I. Frateur, M.E. Orazem, B. Tribollet, The global and local impedance response of a blocking disk electrode with local constant-phase-element behavior, J. Electrochem. Soc. 154 (2007) C89, doi:10.1149/1.2398889.
[35] J.-.B. Jorcin, M.E. Orazem, N. Pébère, B. Tribollet, CPE analysis by local electrochemical impedance spectroscopy, Electrochim. Acta 51 (2006) 1473–1479, doi:10.1016/j.electacta.2005.02.128.
[36] A.J. Bard, M.V. Mirkin, Scanning Electrochemical Microscopy, CRC Press, 2012.
[37] A.G. Marques, M.G. Taryba, A.S. Panão, S.V. Lamaka, A.M. Simões, Application of scanning electrode techniques for the evaluation of iron-zinc corrosion in nearly neutral chloride solutions, Corros. Sci. 104 (2016) 123–131, doi:10.1016/j.corsci.2015.12.002.
[38] J.S. Clemente, P.M. Fedorak, A review of the occurrence, analyses, toxicity, and biodegradation of naphthenic acids, Chemosphere 60 (2005) 585–600, doi:10.1016/j.chemosphere.2005.02.065.
[39] M.A. Deyab, H.A.A. Dief, E.A. Eissa, A.R. Taman, Electrochemical investigations of naphthenic acid corrosion for carbon steel and the inhibitive effect by some ethoxylated fatty acids, Electrochim. Acta 52 (2007) 8105–8110, doi:10.1016/j.electacta.2007.07.009.
[40] H. Namduri, S. Nasrazadani, Quantitative analysis of iron oxides using Fourier transform infrared spectrophotometry, Corros. Sci. 50 (2008) 2493–2497, doi:10.1016/j.corsci.2008.06.034.

[41] W. Xiao, A.M. Jones, R.N. Collins, M.W. Bligh, T.D. Waite, Use of Fourier transform infrared spectroscopy to examine the Fe(II)-catalyzed transformation of ferrihydrite, Talanta 175 (2017) 30–37, doi:10.1016/j.talanta.2017.07.018.
[42] K.D. Efird, R.J. Jasinski, Effect of the crude oil on corrosion of steel in crude oil/brine production, Corrosion 45 (1989) 165–171, doi:10.5006/1.3577835.
[43] B. Smith, Infrared Spectral Interpretation: A Systematic Approach, 1st ed., CRC Press, 2018, doi:10.1201/9780203750841.
[44] F. Echeverría, D. Peña, C. Vásquez, Measurement of electrode potential in oil in water emulsions, Rev. Fac. de Ing. (30) (2003) 78–88, https://revistas.udea.edu.co/index.php/ingenieria/article/view/327315.
[45] R. Skartlien, A. Bertheussen, S. Simon, J. Sjoblom, Development of electrochemical DPD molecular simulations for oil/water partitioning of organic acids at varying pH, J. Dispers. Sci. Technol. 39 (2018) 1367–1375, doi:10.1080/01932691.2017.1404471.
[46] M.A. Ghanem, F. Marken, Mesoporous platinum hosts for electrode|liquid|liquid-Triple phase boundary redox systems, Electrochem. Commun. 7 (2005) 1333–1339, doi:10.1016/j.elecom.2005.09.013.
[47] T.E. Havre, J. Sjöblom, J.E. Vindstad, Oil/water-partitioning and interfacial behavior of naphthenic acids, J. Dispers. Sci. Technol. 24 (2003) 789–801, doi:10.1081/DIS-120025547.
[48] M.P. Barrow, L.A. McDonnell, X. Feng, J. Walker, P.J. Derrick, Determination of the nature of naphthenic acids present in crude oils using nanospray Fourier transform ion cyclotron resonance mass spectrometry: the continued battle against corrosion, Anal. Chem. 75 (2003) 860–866, doi:10.1021/ac020388b.
[49] A. Bertheussen, S. Simon, J. Sjoblom, Equilibrium partitioning of naphthenic acid mixture, Part 1: commercial naphthenic acid mixture, Energy Fuels 32 (2018) 7519–7538, doi:10.1021/acs.energyfuels.8b01494.
[50] A.C. Scott, R.F. Young, P.M. Fedorak, Comparison of GCMS-and FTIR methods for quantifying naphthenic acids in water samples, Chemosphere 73 (2008) 1258–1264, doi:10.1016/j.chemosphere.2008.07.024.
[51] E.D. Bloch, W.L. Queen, R. Krishna, J.M. Zadrozny, C.M. Brown, J.R. Long, Hydrocarbon separations in a metal-organic framework with open iron (II) coordination sites, Science 335 (2012) 1606–1610, doi:10.1126/science.1217544.
[52] M.H. Mohamed, L.D. Wilson, K.M. Peru, J.V. Headley, Colloidal properties of single component naphthenic acids and complex naphthenic acid mixtures, J. Colloid Interface Sci. 395 (2013) 104–110, doi:10.1016/j.jcis.2012.12.056.